Increased Importance of Aerosol-Cloud Interaction for Surface $PM_{2.5}$ Pollution Relative to Aerosol-Radiation Interaction in China with the Anthropogenic Emission Reduction

Da Gao[1, 2], Bin Zhao[1, 2, *], Shuxiao Wang[1, 2], Yuan Wang[3], Brian Gaudet[4], Yun Zhu[5], Xiaochun Wang[1, 2], Jiewen Shen[1, 2], Shengyue Li[1, 2], Yicong He[1, 2], Dejia Yin[1, 2], Zhaoxin Dong[1, 2]

[1]State Key Joint Laboratory of Environment Simulation and Pollution Control, School of Environment, Tsinghua University, 100084 Beijing, China

[2]State Environmental Protection Key Laboratory of Sources and Control of Air Pollution Complex, Beijing, 100084, China

[3]Department of Earth System Science, Stanford University, Stanford, CA, USA

[4]Pacific Northwest National Laboratory, Richland, Washington, USA

[5]Guangdong Provincial Key Laboratory of Atmospheric Environment and Pollution Control, College of Environment and Energy, South China University of Technology, Guangzhou Higher Education Mega Center, Guangzhou, 510006, China

*Correspondence to: Bin Zhao (bzhao@mail.tsinghua.edu.cn)

Abstract: Surface fine particulate matter ($PM_{2.5}$) pollution can be enhanced by feedback processes induced by aerosol-radiation interactions (ARI) and aerosol-

cloud interactions (ACI). Many previous studies have reported enhanced $PM_{2.5}$ concentration induced by ARI and ACI for episodic events in China. However, few studies have examined the changes in the ARI- and ACI-induced $PM_{2.5}$ enhancements over a long period, though the anthropogenic emissions have changed substantially in the last decade. In this study, we quantify the ARI- and ACI-induced $PM_{2.5}$ changes for 2013–2021 under different meteorology and emission scenarios using the Weather Research and Forecasting model with Chemistry (WRF-Chem) and investigate the driving factors for the changes. Our results show that in January 2013, when China suffered from the worst $PM_{2.5}$ pollution, the $PM_{2.5}$ enhancement induced by ARI in eastern China (5.59 μg m^{-3}) is larger than that induced by ACI (3.96 μg m^{-3}). However, the ACI-induced $PM_{2.5}$ enhancement shows a significantly smaller decrease ratio (51%) than the ARI-induced enhancement (75%) for 2013–2021, making ACI more important for enhancing $PM_{2.5}$ concentrations in January 2021. Our analyses suggest that the anthropogenic emission reduction plays a key role in this shift. Owing to only anthropogenic emission reduction, the ACI-induced $PM_{2.5}$ enhancement decreases by 43% in January, lower than the decrease ratio of the ARI-induced enhancement (57%). The relative change in ARI- and ACI-induced $PM_{2.5}$ enhancement in July is similar to the pattern observed in January caused by anthropogenic emission reduction. The primary reason for this phenomenon is that the decrease of ambient $PM_{2.5}$ for 2013–2021 causes a disproportionately small decrease of liquid water path (LWP) and increase of cloud effective radius

(Re) under the condition of high $PM_{2.5}$ concentration. Therefore, the surface solar radiation attenuation (and hence boundary layer height reduction) caused by ACI decreases slower than that caused by ARI. Moreover, the lower decrease ratio of the ACI-induced $PM_{2.5}$ enhancement is dominated by the lower decrease ratio of ACI-induced secondary $PM_{2.5}$ component enhancement, which is additionally caused by smaller decrease ratio of the air temperature reduction and relative humidity (RH) increase. Our findings indicate that, with the decrease of ambient $PM_{2.5}$, the ACI-induced $PM_{2.5}$ enhancement inevitably becomes more important. This needs to be considered in the formulation of control policies to meet the national $PM_{2.5}$ air quality standard.

1. Introduction

Aerosol-radiation interaction (ARI) and aerosol-cloud interaction (ACI) are important ways for aerosols to influence the climate (Rosenfeld et al., 2014; Seinfeld et al., 2016; Liu et al., 2018; Bellouin et al., 2020; Forster et al., 2021). The ARI represents the direct scattering and absorption of solar and infrared radiation by atmospheric aerosols; the ACI denotes the modification effects on the lifetime, physical and optical properties of clouds by atmospheric aerosols.

Previous studies have documented that both ARI and ACI have important contributions to inhibiting the planetary boundary layer height (PBLH), cooling the near-surface air temperature, and increasing the relative humidity (RH) (Wang et al., 2014; Ding et al., 2016; Liu et al., 2018). Moreover, ACI has extra contributions to changing precipitation and cloud chemistry (Zhao et al., 2017;

Zhang et al., 2018). These feedbacks and changes are mostly conducive to increasing the haze severity (Wang et al., 2015; Zhang et al., 2018; Liu et al., 2018; Zhou et al., 2019; Zhang et al., 2020; Xiong et al., 2022; Lin et al., 2022). So far, numerous studies have evaluated the fine particulate matter ($PM_{2.5}$) enhancements caused by the decreases of downward shortwave radiation at the surface (SWDOWN), PBLH, near-surface air temperature and precipitation, and by the increase of RH, especially during the severe $PM_{2.5}$ pollution in China (Le et al., 2020). Zhang et al. (2015) and Zhang et al. (2018) quantified that the ARI caused the $PM_{2.5}$ increase by 8.3 μg m^{-3} in 2013 and 4.0 μg m^{-3} in 2014. However, both positive and negative contributions of ACI to the $PM_{2.5}$ have been revealed (Forkel et al., 2012; 2015; Kong et al., 2015; Zhang et al., 2015; Zhang et al., 2018). Zhao et al. (2017) pointed out that the negative contribution of ACI shown in some studies (Gustafson et al., 2007; Gong et al., 2015) is due to the relatively high prescribed values of cloud droplet number concentration (CDNC) or cloud condensation nuclei (CCN), which could not represent a rather clean condition. Besides, there might be a discrepancy between the enhancements induced by ARI and ACI for primary and secondary $PM_{2.5}$ components. The primary $PM_{2.5}$ components are mainly influenced by physical transport, while the secondary $PM_{2.5}$ components are also affected by chemical formation and decomposition. The lower air temperature and higher RH can help to condense gas precursors into secondary aerosol particles (Donahue et al., 2012) and strengthen aqueous and heterogeneous reactions (Liu et al., 2018). On the contrary, Wu et al. (2020)

pointed out that the ARI may also suppress the formation of secondary aerosol because the atmospheric oxidizing capacity and photolysis rate can be changed during the scattering and absorbing of solar radiation. Therefore, not all changes of meteorological factors are conducive to the increase of secondary $PM_{2.5}$, and these positive and negative contributions would influence the variations of primary and secondary $PM_{2.5}$ components. In a word, although the ARI and ACI processes mostly lead to a net $PM_{2.5}$ increase, the relative increasing rates of different aerosol components are fairly complex due to various physical and chemical processes.

In recent years, the Chinese government has successively proclaimed the policies of "Air pollution prevention and control action plan" and "Three-year action plan to win the blue sky defense war", including the promotion of ultra-low emission technologies in industrial sectors, the implementation of traffic restriction policies, and the transition from coal to gas in residential cooking. As a result, the annually averaged $PM_{2.5}$ concentrations in Beijing-Tianjin-Hebei region, Yangtze River Delta (YRD) and Pearl River Delta have been reduced by 39.6%, 34.2%, and 27.7% from 2013 to 2017, respectively (Wang et al., 2017; Ding et al., 2019a). Meanwhile, sulfate and organic components have respectively decreased by 76% and 70 % in the North China Plain (NCP) (Wang et al., 2019). Considering the sharp anthropogenic emission reduction and $PM_{2.5}$ concentration decrease, Moch et al. (2022) found that the decrease in mean $PM_{2.5}$ concentration from the winter months of 2012–2013 to the winter months of 2016–2017 in

China weakened the cloud–snowfall–albedo feedback induced by the aerosol semi-direct effect. For air quality, Zhang et al. (2022) found that the decrease in black carbon from 2013 to 2017 in China reduced the enhanced $PM_{2.5}$ concentration induced by the ARI by 1.8 μg m^{-3} in January and 0.3 μg m^{-3} in July.

However, none of the previous studies have systematically evaluated the changes in enhanced $PM_{2.5}$ concentrations through ARI and ACI in China at the long-term scale. Besides, the driving force and physical mechanisms for the changes are also yet to be explored. In this study, we try to investigate the enhanced $PM_{2.5}$ concentrations induced by ARI and ACI in 2013 over China, the impact of the changes in the meteorological background and anthropogenic emission from 2013 to 2021 on ARI- and ACI-induced $PM_{2.5}$ enhancements and its components. Furthermore, the causes of $PM_{2.5}$ enhancement changes are analyzed.

2. Model and experimental design

2.1 Model configuration

The Weather Research and Forecasting model with Chemistry (WRF-Chem) version 4.2 has been used in this study. The model domain covers the whole land area of China with a horizontal resolution of 27 km × 27 km. There are 24 vertical layers from surface to 50 hPa, with denser layers in the planetary boundary layer (PBL). Major physical options used in the model include the Morrison double-

moment scheme (Morrison et al., 2009), the Rapid Radiative Transfer Model for GCMs (RRTMG) shortwave and longwave radiative transfer schemes (Iacono et al., 2008), the Eta similarity surface-layer scheme (Janjic et al., 1994), the Noah land-surface model with multiple parameterization options (Niu et al., 2011), the Bougeault and Lacarrere PBL scheme (Bougeault et al., 1989), and the Grell-Freitas ensemble cumulus scheme (Grell et al., 2014). For chemistry, we employ the SAPRC-99 (Statewide Air Pollution Research Center mechanism, version 1999) as the gas-phase chemistry mechanism (Carter et al., 2000). The aerosol module used in the study is the Model for Simulating Aerosol Interactions and Chemistry (MOSAIC) (Zaveri et al., 2008), which includes all major aerosol processes and represents the aerosol size distribution with 8 size bins. The MOSAIC also incorporates the one-dimensional Volatility Basis Set (VBS) framework that improves the simulation of secondary organic aerosol (Shrivastava et al., 2011). Rates for photolytic reactions are calculated using the Fast-J photolysis rate scheme (Wild et al., 2000). Additionally, we noted the poor ability of nitrate simulation in the WRF-Chem model. We improved the nitrate simulation by addressing the HONO underestimation in the model (Wang et al., 2015; Xue et al., 2020). More detailed information can be found in Section 1 in the Supplementary Information. The meteorological initial and boundary conditions are derived from the National Centers for Environmental Prediction Final Analysis reanalysis data with resolutions of 1.0° × 1.0° and 6 h (*http://rda.ucar.edu/datasets/ds083.2/*). The chemical initial and boundary

conditions are acquired from the simulation results of the National Center for Atmospheric Research's Community Atmosphere Model with Chemistry (CAM-Chem, before 2020, *https://www.acom.ucar.edu/cam-chem/cam-chem.shtml*) and the Whole Atmosphere Community Climate Model (WACCM, after 2020, *https://www.acom.ucar.edu/waccm/download.shtml*) with resolutions of 0.94° × 1.25° and 6 h.

The anthropogenic emission data in China for 2013-2021 are obtained from the ABaCAS-EI (Air Benefit and Cost and Attainment Assessment System-Emission Inventory) developed by Tsinghua University (Li et al., 2023). Specific emissions of SO_2, NO_x (NO and NO_2), NH_3, $PM_{2.5}$ and VOCs in 2013 and 2021 are presented in Table S2. The emission data in other countries are obtained from the IIASA emission inventory for 2015 (Zheng et al., 2019; Gao et al., 2020). The biogenic emission is calculated online by the Model of Emissions of Gases and Aerosols from Nature (MEGAN) v2.04 (Guenther et al., 2006). The dust emission is calculated online by the Goddard Chemistry Aerosol Radiation and Transport (GOCART) model coupled with the MOSAIC aerosol schemes. (Zhao et al., 2010; 2013)

To account for the physical processes of aerosol-radiation-cloud feedback on meteorological factors and $PM_{2.5}$, the four-dimensional data assimilation (FDDA) is not utilized in our simulations. Aerosol optical depth, single scattering albedo, and asymmetry factors are calculated based on the Lorenz-Mie theory as a function of wavelength and three-dimensional location (Fast et al., 2006). Then,

the aerosol optical properties are transferred to the RRTMG radiation scheme to calculate the impact of aerosol on the radiation balance (Iacono et al., 2008). As for the ACI, activated aerosols are calculated by the Abdul-Razzak and Ghan scheme (Abdul-Razzak & Ghan, 2002) and are then coupled with the Morrison two-moment cloud microphysics scheme (Morrison et al., 2009). The prognostic cloud water content calculated by the Morrison scheme is input into the RRTMG scheme for the radiative transfer calculation. It should be noted that the prognostic aerosol does not influence cumulus clouds and ice nucleation in the model. The prognostic aerosol can only be activated as CCN. It does not directly contribute to ice nucleation, which is only influenced by air temperature and supersaturation (Kanji et al., 2017). Furthermore, CCN would influence grid-scale clouds. However, limited by the horizontal resolution of 27 km × 27 km, cumulus clouds could not be resolved in this grid.

2.2 Experimental design

As described in the introduction, the purpose of this study is to quantify the contributions of ARI and ACI to $PM_{2.5}$ concentrations under different emission scenarios. The simulation periods are January and July, 2013 and 2021, representing winter and summer, respectively.

As shown in Table 1, the enhanced $PM_{2.5}$ concentration induced by ARI and ACI could be obtained via comparing the simulation results with ARI or ACI turned on or off. By setting the 'aer_ra_feedback' to 0 in the model, the ARI could

be turned off, which means that the interaction between aerosol and radiation is prevented. The ACI could be turned off through prescribing the CDNC of 25 cm^{-3} in the microphysical scheme, which represents average level in the pristine air (Bennartz et al., 2007). For example, the 13M13E_B, 13M13E_NR and 13M13E_NRC shown in Table 1 represent the cases with ARI and ACI effects, without ARI effect, and without ARI and ACI effects in 2013, respectively. The ARI-induced $PM_{2.5}$ enhancement could be acquired by comparing the results of 13M13E_B and 13M13E_NR; the ACI-induced $PM_{2.5}$ enhancement could be obtained by comparing the results of 13M13E_NR and 13M13E_NRC.

Table 1. Case definition under different meteorological backgrounds and anthropogenic emissions with ARI or ACI turned on or off.

Case	Meteorology	Emission	ARI	ACI
13M13E_B	Jan & Jul, 2013	Jan & Jul, 2013	on	on
13M13E _NR	Jan & Jul, 2013	Jan & Jul, 2013	off	on
13M13E _NRC	Jan & Jul, 2013	Jan & Jul, 2013	off	off
21M13E_B	Jan & Jul, 2021	Jan & Jul, 2013	on	on
21M13E_NR	Jan & Jul, 2021	Jan & Jul, 2013	off	on
21M13E_NRC	Jan & Jul, 2021	Jan & Jul, 2013	off	off
21M21E_B	Jan & Jul, 2021	Jan & Jul, 2021	on	on
21M21E_NR	Jan & Jul, 2021	Jan & Jul, 2021	off	on
21M21E_NRC	Jan & Jul, 2021	Jan & Jul, 2021	off	off

In order to obtain the changes of the ARI- and ACI-induced $PM_{2.5}$ enhancements from 2013 to 2021 caused by the variation of meteorological background and by the reduction of anthropogenic emission, the control experiments (21M13E; three experiments: with ARI and ACI turned on, with ARI turned off and ACI turned on, and with ARI and ACI turned off) are designed with the meteorological background in 2021 and the anthropogenic emission in 2013. In the following, the 13M13E, 21M13E and 21M21E represent the cases with meteorological background and anthropogenic emission in 2013, meteorological background in 2021 and anthropogenic emission in 2013, and meteorological background and anthropogenic emission in 2021, respectively. Taking the ARI for example, the change of the ARI-induced $PM_{2.5}$ enhancement from the variation of meteorological background is obtained by subtracting the ARI-induced $PM_{2.5}$ enhancement in the 13M13E from that in the 21M13E [Eq. (1)]; the change in the ARI-induced $PM_{2.5}$ enhancement from the reduction of anthropogenic emission is obtained by subtracting the ARI-induced $PM_{2.5}$ enhancement in the 21M13E from that in the 21M21E [Eq. (2)]. The calculations for the ACI-induced $PM_{2.5}$ enhancement are similar, as shown in Eqs. (3) and (4).

$$ARI_{met} = (21M13E\_B - 21M13E\_NR) - (13M13E\_B - 13M13E\_NR), \quad (1)$$

$$ARI_{emi} = (21M21E\_B - 21M21E\_NR) - (21M13E\_B -$$

$21M13E\_NR)$, (2)

$ACI_{met} = (21M13E\_NR - 21M13E\_NRC) - (13M13E\_NR - 13M13E\_NRC)$, (3)

$ACI_{emi} = (21M21E\_NR - 21M21E\_NRC) - (21M13E_{NR} - 21M13E_{NRC})$, (4)

where the ARI_{met} (ACI_{met}) and ARI_{emi} (ACI_{emi}) represent the changes of the enhanced $PM_{2.5}$ concentration induced by the ARI (ACI) from 2013 to 2021 caused by the variation of meteorological background and reduction of anthropogenic emission, respectively.

2.3 Model evaluation

To determine the accuracy and reliability of simulation results, the 13M13E_B and 21M21E_B simulations (Table 1) are verified by using the observations. The variables checked in the evaluation contain the concentration and components of surface $PM_{2.5}$ and the meteorological factors, including air temperature (T2) and water vapor mixing ratio (Q2) at 2 m, wind speed (WS10) and wind direction (WD10) at 10 m, as well as cloud fraction (CF) and liquid water path (LWP).

Simulated temperature, wind, and water vapor are compared with the observations from the National Climate Data Center (NCDC, http://www.ncdc.noaa.gov/). The evaluation shows that the absolute errors for T2, WS10 and Q2 are respectively less than 1℃, 1 m s^{-1} and 0.1 g kg^{-1} (Table S3),

and those for WD10 are near or less than 10°. For the simulation utilizing the FDDA, the benchmarks of biases proposed by Emery et al. (2001) are 0.7°C, 0.6 m s^{-1}, 1.0 g kg^{-1} and 20° for the T2, WS10, Q2 and WD10, respectively. The biases of the T2 and WS10 in our simulations have exceeded the benchmarks, while they are still similar to or smaller than in most previous WRF-Chem applications without FDDA over East Asia (Zhang et al., 2015; Zhao et al., 2017).

Simulated CF and LWP are compared with the data from the Moderate-resolution Imaging Spectroradiometer (MODIS) aboard the Terra satellite (http://ladsweb.nascom.nasa.gov/data/search.html). Overall, the CF and LWP simulations are in good agreement with the observations (Figs. S1 and S2). The high values of observed CF and LWP primarily appear in the south of China in January 2013 and 2021, and high value of CF also occurs in the NCP region. The high values of CF and LWP in the south of China could be reproduced in the simulation, while the CF in NCP region is slightly underestimated, which could be owing to imperfect cloud parameterization scheme in the model or uncertainties in the retrieval of MODIS datasets. In July 2013 and 2021, part of high value area of observed LWP and most high value area of observed CF appear in the southwestern China and the east coast of China, which also could be captured by the simulation. In addition, high LWP also appears in Gansu and Sichuan Provinces in July 2013 and in the YRD and Sichuan-Chongqing in July 2021, which are both well reproduced. The distributions of low values of observed CF and LWP in January and July of 2013 and 2021 are also well

simulated.

The simulation of surface $PM_{2.5}$ concentration is compared with the data from the China National Environmental Monitoring Center (*https://quotsoft.net/air/*). The evaluation shows that both the regional average value and spatial distribution of simulated $PM_{2.5}$ concentration are in good agreement with the observational data. As shown in Fig. S3, the biases of regional average $PM_{2.5}$ concentration in January and July of 2013 and 2021 are below 5 $\mu g\ m^{-3}$ in eastern China. In this study, the eastern China includes most of Chinese provinces except Xinjiang, Xizang, Ningxia, Qinghai, Gansu, Inner-Mongolia and Heilongjiang Provinces, which contains most polluted regions in China. In addition, the distributions of high simulated $PM_{2.5}$ concentration are also consistent with the observations, such as the NCP region, the YRD region, and the Sichuan-Chongqing area.

The simulated $PM_{2.5}$ components are also reasonable compared with the observation data. Given that the $PM_{2.5}$ components data in 2013 are very rare, we sourced three sets of data in January 2013, respectively in Beijing (Mattias et al., 2017), Handan (Zhang et al., 2015), and Shanghai (Li et al., 2015). The results show that the simulated $PM_{2.5}$ components are reproduced well generally. Specifically, the simulated $PM_{2.5}$ components are larger than half of observational $PM_{2.5}$ components and less than the double observational $PM_{2.5}$ components (Fig. S4). Observed $PM_{2.5}$ components data in 2021 are from a data sharing platform for the NCP region and its surrounding areas (Wang et al., 2019). Fig. S5 shows

the ratios of observation to simulation of ammonium, sulfate, BC and organic carbon (OC) in January and July 2021. The results exhibit that almost all the ratios of $PM_{2.5}$ components are located between 0.5 and 2.0, while some ratios of sulfate in January, part of OC in January, and BC in January and July are beyond this range. But these discrepancies will not cause obvious uncertainties in this research. Specifically, considering BC low hygroscopicity, BC overestimations in January and July 2021 probably bring low uncertainties in ACI-induced $PM_{2.5}$ enhancement. To test the impact of simulated BC overestimation in January 2021 on ARI-induced $PM_{2.5}$ enhancement, we utilize another set of particulate matter (PM) source profiles (Liu et al., 2018) and conduct the simulations for January 2021. The results indicate that the ratios of simulated BC concentration to observational BC concentration are within 2.0. The ARI-induced $PM_{2.5}$ enhancement is 1.33 μg m^{-3}, which shows a negligible difference from the result (1.37 μg m^{-3}) obtained using original PM source profiles (Fig. S6). In view of the results in January 2021, the BC overestimation in July 2021 also probably brings low uncertainties in ARI-induced $PM_{2.5}$ enhancement. However, the reduction in simulated BC concentration in January 2021 does not necessarily mean that this set of PM source profiles is better than the original PM source profiles, because this might be an accidental result caused by other uncertainties. For example, the current model underestimates the wet deposition of BC due to neglecting the increase in BC hygroscopicity brought about by BC aging. If this process is considered in the model, simulated BC concentrations might be better reproduced

using original PM source profiles. Therefore, in this study, we still use the original results for our analysis. The model also underestimates the sulfate concentration and overestimates the part of OC concentration in January 2021. We think that neither of these discrepancies will cause significant uncertainties in ARI- and ACI-induced $PM_{2.5}$ enhancement. Specifically, the majority of aerosol is scattering aerosol and the $PM_{2.5}$ concentration in January 2021 is reproduced well. Therefore, we think that the impact of the sulfate underestimation on the ARI-induced $PM_{2.5}$ enhancement would be largely offset by the overestimation of other scattering aerosol components, such as OC. In addition, the OC overestimation should not bring significant uncertainty to ACI-induced $PM_{2.5}$ enhancement either, because of the relatively lower hygroscopicity of OC compared to secondary inorganic aerosol. The underestimation of sulfate simulation in January 2021 also minimally affects ACI-induced $PM_{2.5}$ enhancement because the sulfate underestimation mainly occurs in the North China Plain, where cloud cover is low. In contrast, in southern cities such as Mianyang city in Sichuang province where there is plenty of cloud cover, the sulfate simulation was 4.19 μg m^{-3} in January 2021, which is very close to the observed value of 4.25 μg m^{-3} (Lin et al., 2022).

In summary, the performances of WRF-Chem model on the simulations of air quality and meteorological factors over China are fairly good, and the differences between simulations and observations are reasonable and acceptable.

3. Results and discussion

3.1 The impacts of ARI and ACI feedbacks on the meteorological factors and $PM_{2.5}$ concentrations in 2013

We comprehensively discuss the effects of ARI and ACI on the regional meteorological factors and $PM_{2.5}$ concentrations in January and July 2013. Fig. 1 shows the impacts of ARI and ACI feedbacks on the SWDOWN, PBLH, T2, RH and $PM_{2.5}$ concentration in January and July 2013. For the ARI, the SWDOWN decreases by 18.37 and 7.71 W m^{-2} in January and July 2013 in eastern China, respectively. Since the incoming solar radiation reaching the ground is reduced by PM, the T2 and PBLH in eastern China further decrease by 0.30 and 0.03°C, and 28.34 and 8.75 m in January and July 2013, respectively. Meanwhile, the RH increases by 0.46% and 0.08% due to the water vapor accumulation in the suppressed planetary boundary layer (Liu et al., 2018). Ultimately, the $PM_{2.5}$ concentration increases by 5.59 and 0.13 μg m^{-3} in eastern China (Fig. 1d). For the ACI, affected by the cloud modified by the aerosol, the SWDOWN, T2 and PBLH decrease by 7.54 and 14.03 W m^{-2}, 0.18 and 0.17 °C, and 10.89 and 24.31 m, and the RH increases by 0.34% and 0.37% in January and July 2013 in eastern China, respectively. As a result, the $PM_{2.5}$ concentration increases by 3.96 and 2.20 μg m^{-3} in eastern China. Fig. 2 shows that the regional averaged values and spatial distributions of $PM_{2.5}$ enhancements induced by ARI and ACI in 2013 are in line with the results of previous studies (Zhao et al., 2017; Zhang et al., 2018).

Overall, the enhanced $PM_{2.5}$ concentration induced by ARI is greater than

that induced by ACI in January 2013, which is due to the relatively low LWP in the high $PM_{2.5}$ concentration area. But it shows the opposite situation in July 2013, owing to the plentiful cloud in warm July (Zhang et al., 2018).

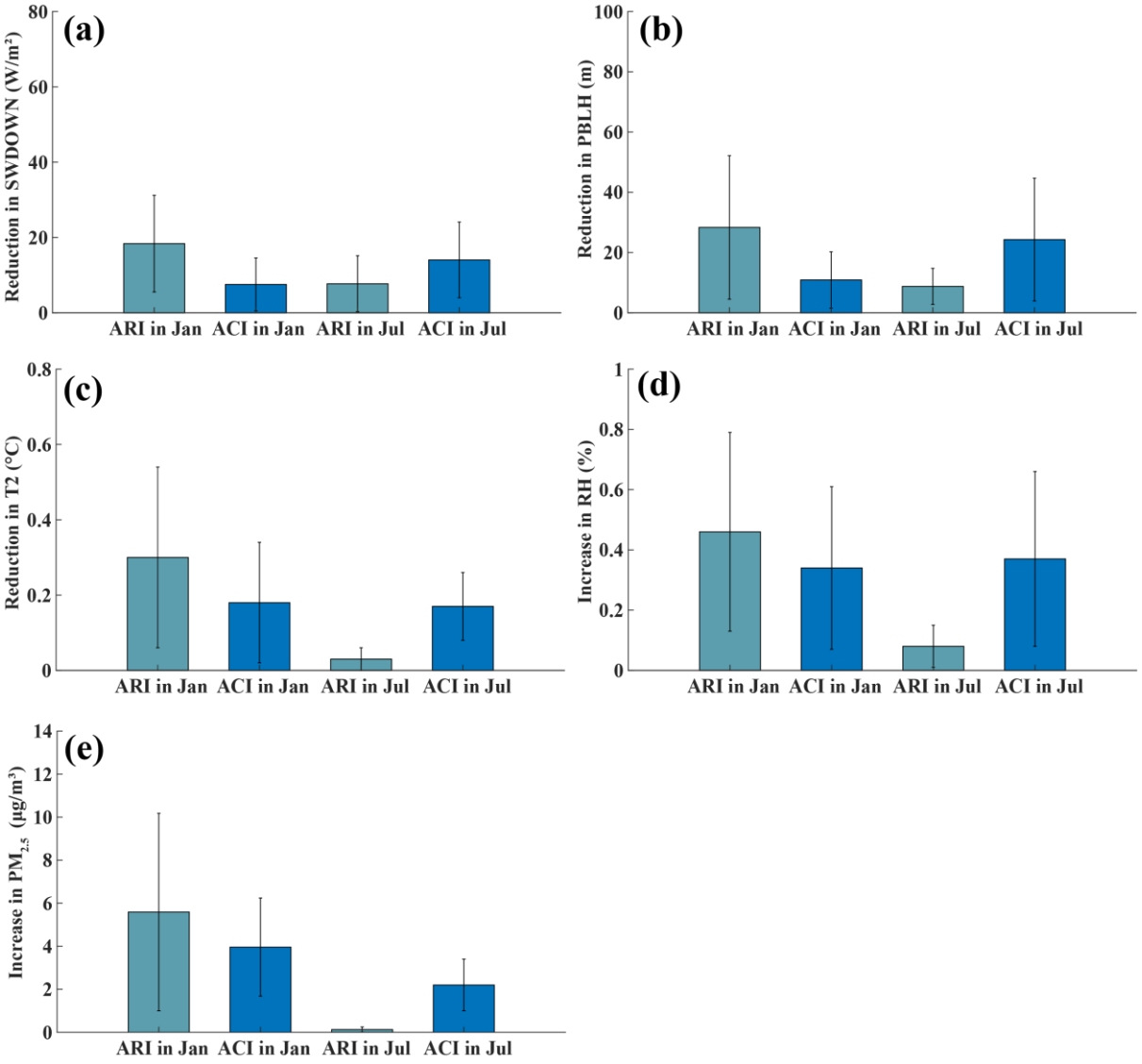

Fig. 1. The regional averaged reductions of (a) downward shortwave radiation at the surface (SWDOWN), (b) planetary boundary layer height (PBLH), (c) 2-m air temperature (T2), and increments of (d) relative humidity (RH) and (e) fine particulate matter ($PM_{2.5}$) concentration induced by the aerosol-radiative interaction (ARI) and aerosol-cloud interaction (ACI) in January and July 2013

in eastern China, the error bars represent the standard deviations for different meteorological factors and $PM_{2.5}$ concentration induced by ARI and ACI in January and July 2013 in eastern China.

3.2 The shift of the $PM_{2.5}$ enhancements induced by ARI and ACI

As discussed in section 3.1, the enhanced $PM_{2.5}$ concentrations induced by ARI and ACI exhibit obvious spatial and seasonal variations in 2013. However, due to the variations of meteorological background and the reduction of anthropogenic emission from 2013 to 2021, their joint and individual impacts on the ARI- and ACI-induced $PM_{2.5}$ enhancements are still unclear. Fig. 2 shows the ARI- and ACI-induced $PM_{2.5}$ enhancements in the experiments of 13M13E, 21M13E and 21M21E in January and July.

As shown in Fig. 2, from 2013 to 2021, the $PM_{2.5}$ concentration enhancement induced by the ARI in January decreases by 75% (from 5.59 to 1.37 μg m^{-3}). Zhang et al. (2022) also found that the ARI effect over China weakens during 2013–2017, and the ratio of $PM_{2.5}$ enhancement to the ambient $PM_{2.5}$ concentration decreases from 5.40% to 3.30%. The decline of the $PM_{2.5}$ enhancement ratio (2.10%) is lower than that in this study (3.26%) due to the continuous emission reduction after 2017. On the other hand, the ACI-induced $PM_{2.5}$ enhancement decreases by 51%, from 3.96 to 1.93 μg m^{-3}. With lower percentage decrease in the $PM_{2.5}$ enhancement, the ACI-induced $PM_{2.5}$ enhancement exceeds the ARI-induced $PM_{2.5}$ enhancement in January 2021. In

July, both the ARI- and ACI-induced $PM_{2.5}$ enhancements show decreasing trends, the percentage decreases of the ARI-induced (31%) and ACI-induced (34%) $PM_{2.5}$ enhancements are very close.

The contributions of the meteorological background variation and anthropogenic emission reduction to the changes of the ARI- and ACI-induced $PM_{2.5}$ enhancements are different. Due to the meteorological background change from 2013 to 2021, the ARI- and ACI-induced $PM_{2.5}$ enhancements show different characteristics in January and July. It can be seen that, the ARI-induced $PM_{2.5}$ enhancement decreases from 5.59 to 3.15 μg m^{-3} with the variation of meteorological background in January, while it increases from 0.13 to 0.27 μg m^{-3} in July. The primary reason for the difference is that the ambient $PM_{2.5}$ concentration decreases in January but increases in July caused by different meteorological backgrounds. The ACI-induced $PM_{2.5}$ enhancement changes slightly from 3.96 to 3.40 μg m^{-3} in January due to the variation of meteorological background. However, it increases from 2.20 to 3.31 μg m^{-3} in July, because of a large aerosol-induced LWP increase in July 2021.

Considering the reduction of anthropogenic emission, the ARI- and ACI-induced $PM_{2.5}$ enhancements both show declining trends (middle and right columns in Fig. 2). The ARI-induced $PM_{2.5}$ enhancement decreases by 56.51% in January, from 3.15 to 1.37 μg m^{-3}. The ACI-induced $PM_{2.5}$ enhancement decreases by 43.24%, from 3.40 to 1.93 μg m^{-3}. The percentage decrease of the ACI-induced $PM_{2.5}$ enhancement is lower than that of the ARI-induced in January,

which also occurs in July, when the ARI-induced $PM_{2.5}$ enhancement decreases by 66.67% (from 0.27 to 0.09 μg m^{-3}) and ACI-induced $PM_{2.5}$ enhancement decreases by 56.50% (from 3.31 to 1.44 μg m^{-3}).

In summary, both the variation of meteorological background and the reduction of anthropogenic emission play important roles in changing the ARI- and ACI-induced $PM_{2.5}$ enhancements. However, the decreases of ARI- and ACI-induced $PM_{2.5}$ enhancements from 2013 to 2021 are primarily attributed to the reduction of anthropogenic emission. In addition, the percentage decrease of the ACI-induced $PM_{2.5}$ enhancement is lower than that induced by the ARI in both January and July. Therefore, the ACI-induced $PM_{2.5}$ enhancement has become increasingly important in both January and July from 2013 to 2021.

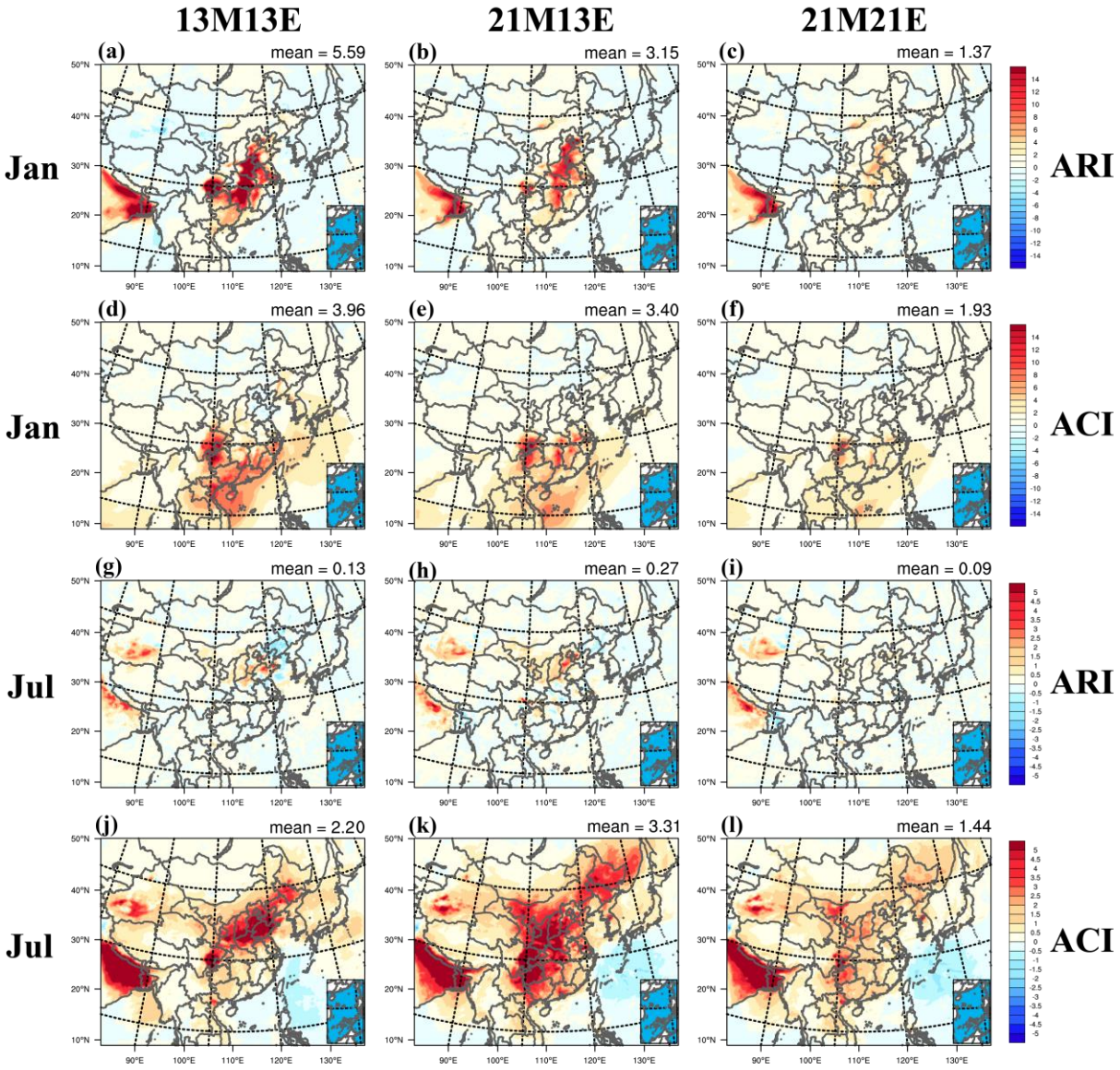

Fig. 2. The distributions of enhanced $PM_{2.5}$ concentrations (unit: μg m^{-3}) induced by the ARI (first and third rows) and the ACI (second and fourth rows) in January (first and second rows) and July (third and fourth rows) in the experiments of 13M13E (left column), 21M13E (middle column) and 21M21E (right column).

3.3 The changes in the enhanced $PM_{2.5}$ components induced by the ARI and the ACI

In terms of the anthropogenic emission reduction, the percentage decrease

of the ACI-induced $PM_{2.5}$ enhancement is lower than that induced by the ARI in both January and July. We find that the difference is primarily from the different percentage decreases of the secondary $PM_{2.5}$ component enhancements induced by ARI and ACI.

Fig. 3 shows the percentage decreases of ARI- and ACI-induced $PM_{2.5}$ component enhancements caused by the anthropogenic emission reduction in January and July. It can be seen that the difference between the percentage decreases of the ARI- and ACI-induced enhancements of sulfate, nitrate, ammonium and OC is larger than those of BC and other inorganic aerosol (OIN). OIN refers to inorganic compositions other than sulfate, nitrate, ammonium, and BC. These compositions include sea salt and mineral elements. Specifically, the difference between the percentage decreases for sulfate, nitrate, ammonium and OC enhancements are 34.66%, 40.20%, 13.80% and 25.65% respectively, and the values for OIN and BC are 8.67% and 6.67%. This result indicates that the lower decrease in the ACI-induced $PM_{2.5}$ concentration enhancement is mainly due to the small decrease in the ACI-induced enhancements of secondary $PM_{2.5}$ components. The main causes will be illustrated in section 3.4.

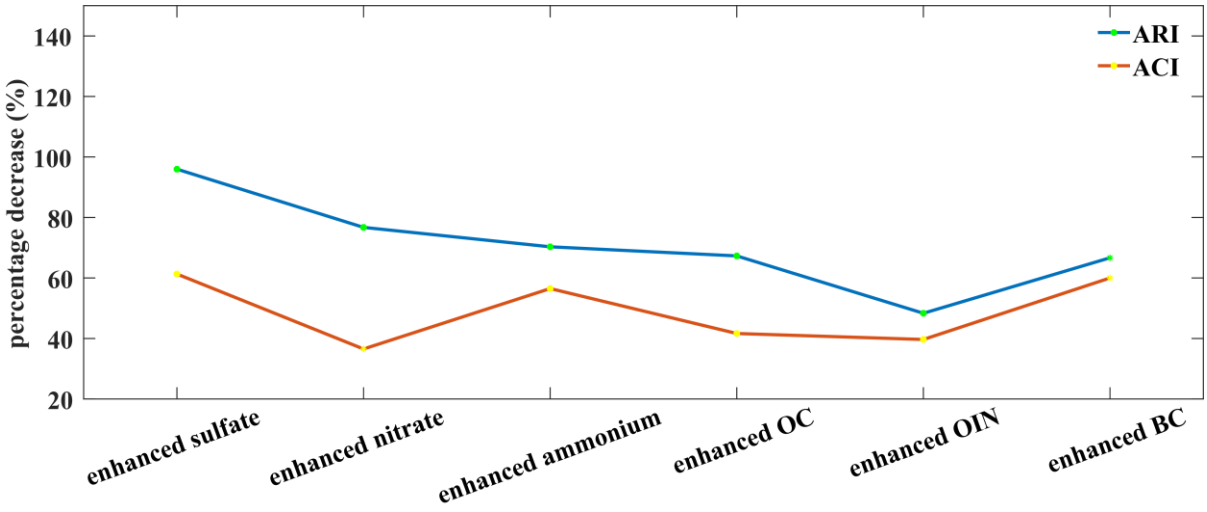

Fig. 3. Percentage decreases (21M13E−21M21E)/21M13E) of the spatial and temporal average ARI- and ACI-induced $PM_{2.5}$ component enhancements in eastern China in January and July caused by the anthropogenic emission reduction from 2013 to 2021.

3.4 Causes for the increased importance of ACI

3.4.1 Explanation from the perspective of meteorological changes

As discussed in previous studies, the decrease of PBLH and T2 and the increase of RH are tightly related to the ARI- and ACI-induced $PM_{2.5}$ enhancements (Donahue et al., 2012; Ding et al., 2016; Moch et al., 2022; Liu et al., 2018). From the perspective of the ARI- and ACI-induced changes in meteorological factors, we investigate the primary reasons for the increasing importance of the ACI-induced $PM_{2.5}$ enhancement under the reduction of anthropogenic emission.

Fig. 4 shows the percentage decreases of ARI- and ACI-induced decrease of SWDOWN, PBLH and T2 and increase of RH due to the reduction of

anthropogenic emission from 2013 to 2021. In January, in order to illustrate the reasons of the lower percentage decrease in the ACI-induced $PM_{2.5}$ enhancement clearly, we take the highly polluted NCP region as an example. As shown in Fig. 4c, the percentage decreases of the ACI-induced decline of SWDOWN (19%), PBLH (27%) and T2 (20%) and the increase of RH (24%) are lower than those of the ARI-induced decline of SWDOWN (29%), PBLH (39%) and T2 (32%) and the increase of RH (36%). The phenomenon in July is similar with that in January (Figs. 4a and b). To our knowledge, the PBLH and T2 are determined by the incoming solar radiation at the surface, and they can strongly influence the RH. So the lower percentage decrease in the ACI-induced reductions of PBLH and T2 and increase of RH could be explained by the lower percentage decrease in the ACI-induced SWDOWN reduction.

We believe that the relatively lower decrease in the ACI-induced SWDOWN reduction is inevitable under high ambient $PM_{2.5}$ concentration. As shown in Fig. S8b, the SWDOWN reduction induced by the ARI shows a linear relationship with the decline of ambient $PM_{2.5}$ concentration, which is similar with Zhou et al. (2018). In contrast, the decrease in the SWDOWN reduction induced by the ACI is lower than that by the ARI due to the ambient $PM_{2.5}$ decrease in the high $PM_{2.5}$-polluted regime. The reason is that the decrease in ambient $PM_{2.5}$ concentration directly weakens the ARI-induced SWDOWN reduction, but it has only a minor impact on the ACI-induced SWDOWN reduction because the change in LWP and cloud effective radius (Re) induced by ACI is not sensitive to $PM_{2.5}$ reduction in

the $PM_{2.5}$-polluted regime. In our simulations, the influence of ACI-induced Re change is relatively smaller than that of ACI-induced LWP change with a large decrease in $PM_{2.5}$ concentration (Fig. S7). Therefore, we are only concerned with change in ACI-induced LWP with a reduction in $PM_{2.5}$. As shown in Fig. S8a, when the ambient $PM_{2.5}$ concentration exceeded 15 μg m^{-3}, the decrease in ACI-induced LWP increase is relatively low with a $PM_{2.5}$ reduction from 120 to 15 μg m^{-3}, indicating that aerosols are not a key limiting factor to cloud formation in this range. Note that when the ambient $PM_{2.5}$ concentration decreases to 15 μg m^{-3}, the weakening of SWDOWN reduction induced by the ACI might be larger than that by the ARI. This is because decrease in ACI-induced LWP increase is relatively fast, with a $PM_{2.5}$ reduction from 15 to 0 μg m^{-3}. Previous studies have demonstrated that the decrease in ACI-induced LWP increase is relatively fast or slow with the ambient $PM_{2.5}$ reduction in the $PM_{2.5}$-clean or polluted condition, respectively (Myhre et al., 2007; Savane et al., 2015). The regional and temporal average $PM_{2.5}$ concentration in eastern China in January and July simulated using background meteorology in 2021 and emissions in 2013 is 63 and 25 μg m^{-3}, which is much higher than 15 μg m^{-3}. Therefore, the decrease in ACI-induced SWDOWN reduction in both months is weak.

Especially, the lower PBLH caused by ARI and ACI will enhance the accumulation of all the $PM_{2.5}$ components, but higher RH and lower T2 induced by the ARI and ACI could promote the production of extra secondary $PM_{2.5}$ components through strengthening aqueous and heterogeneous reactions and

causing gas precursors to condense into particle matter (Donahue et al., 2012; Liu et al., 2018). Therefore, lower percentage decrease in the T2 reduction and RH increase induced by the ACI is more likely to weaken the decrease in the enhancements of secondary $PM_{2.5}$ components. This well explains the lower percentage decreases in the enhancements of secondary $PM_{2.5}$ components induced by the ACI than those by the ARI as shown in Fig. 3.

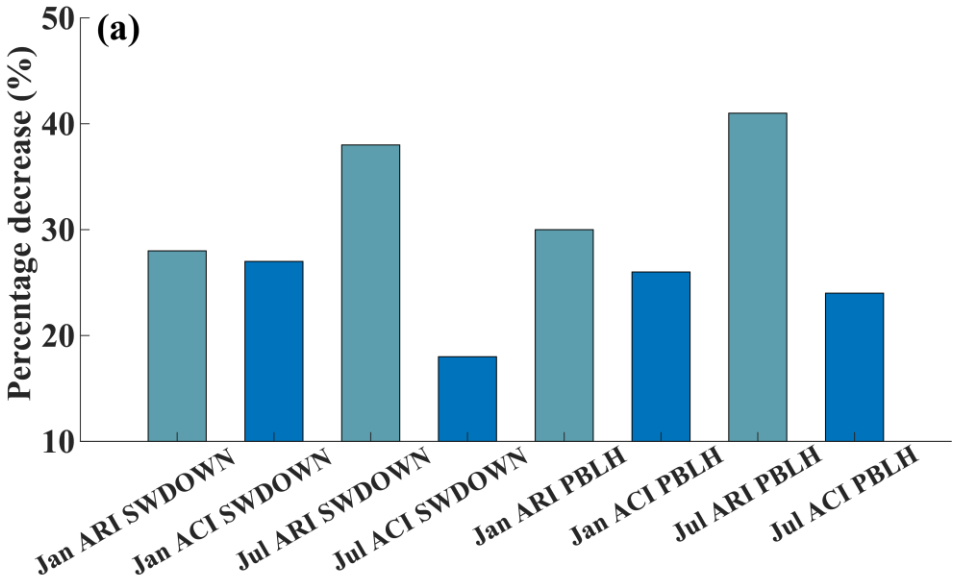
(a)
Percentage decrease (%)
50
40
30
20
10
Jan ARI SWDOWN
Jan ACI SWDOWN
Jul ARI SWDOWN
Jul ACI SWDOWN
Jan ARI PBLH
Jan ACI PBLH
Jul ARI PBLH
Jul ACI PBLH

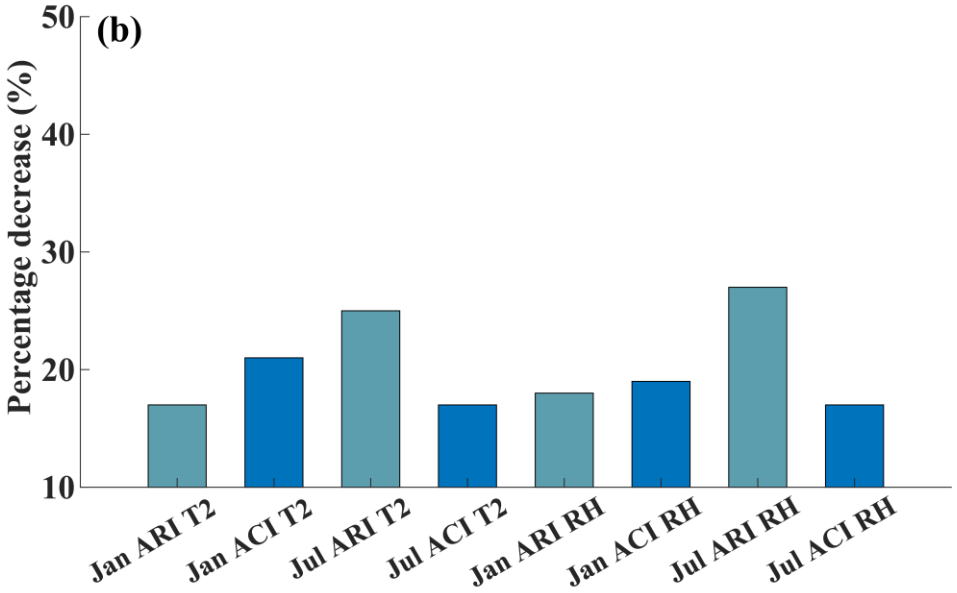
(b)
Percentage decrease (%)
50
40
30
20
10
Jan ARI T2
Jan ACI T2
Jul ARI T2
Jul ACI T2
Jan ARI RH
Jan ACI RH
Jul ARI RH
Jul ACI RH

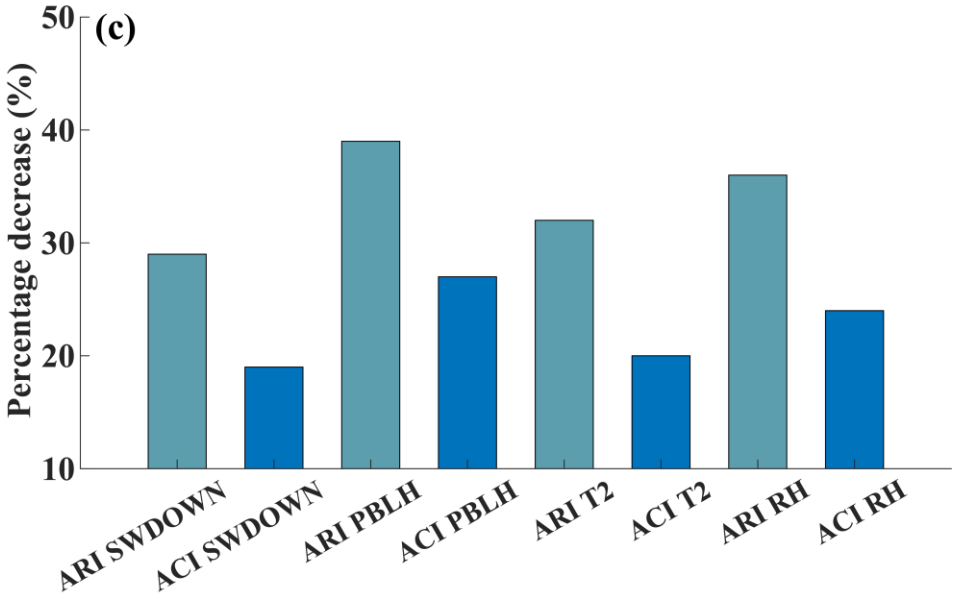
(c)
Percentage decrease (%)
50
40
30
20
10
ARI SWDOWN
ACI SWDOWN
ARI PBLH
ACI PBLH
ARI T2
ACI T2
ARI RH
ACI RH

519

Fig. 4. The percentage decreases of the regional averages of (a) the decrease of SWDOWN and PBLH, and (b) the T2 reduction and RH increase induced by ARI and ACI in eastern China caused by the anthropogenic emission reduction in January and July from 2013 to 2021. (c) is the same as (a) and (b), but in the NCP region in January.

3.4.2 Explanation from the perspective of $PM_{2.5}$ concentration distribution changes

Ambient $PM_{2.5}$ concentration is the fundamental factor to trigger the ARI and the ACI. In order to further explore the reasons for the increasing importance of enhanced $PM_{2.5}$ concentration induced by ACI, we discuss the characteristics of enhanced $PM_{2.5}$ concentration induced by ARI and ACI under different $PM_{2.5}$ pollution levels. Given that this study mainly focuses on the change in ARI- and ACI-induced $PM_{2.5}$ enhancement in the $PM_{2.5}$-polluted regime. we only discuss these changes within the $PM_{2.5}$ concentration range of 15–180 μg m^{-3}

The $PM_{2.5}$ concentration is divided into 11 levels from 15 to 180 μg m^{-3}. As shown in Fig. 5a, in the heavily $PM_{2.5}$-polluted regime (135–180 μg m^{-3}), the decrease in SWDOWN induced by ARI is much larger than that induced by ACI (Fig. S9a). Then, the decrease in PBLH and T2 and the increase in RH induced by ARI are also larger than those induced by ACI (Fig. S9b–d). Thus, the enhanced $PM_{2.5}$ induced by the ARI is much larger than that by the ACI (Fig. 5a). However, when the $PM_{2.5}$ concentration decrease to the range of 15–45 μg m^{-3},

the decrease in SWDOWN, PBLH, and T2 and the increase in RH induced by ACI significantly exceed those induced by ARI. Thus, the ACI-induced $PM_{2.5}$ enhancement significantly exceeds the ARI-induced $PM_{2.5}$ enhancement and becomes more important. This indicates the fast decrease in the ARI-induced $PM_{2.5}$ enhancement and the increasing contribution of the ACI-induced $PM_{2.5}$ enhancement with the decrease in the $PM_{2.5}$ concentration. In summary, the percentage decrease in the $PM_{2.5}$ enhancement induced by ACI is weaker than that induced by ARI with the decrease of $PM_{2.5}$ concentration because of the lower percentage decrease in the ACI-induced SWDOWN, which causes the lower percentage decrease in the ACI-induced PBLH and T2 reduction and the RH increase. Furthermore, as shown in Fig. S8a, the low percentage decrease in the ACI-induced SWDOWN reduction is due to a low decrease in the ACI-induced LWP in the $PM_{2.5}$-polluted regime. Considering the decrease in the ambient $PM_{2.5}$ concentration due to the anthropogenic emission reduction from 2013 to 2021 (Fig. 5b), the ACI-induced $PM_{2.5}$ enhancement certainly contributes more to the total $PM_{2.5}$ concentration in 2021.

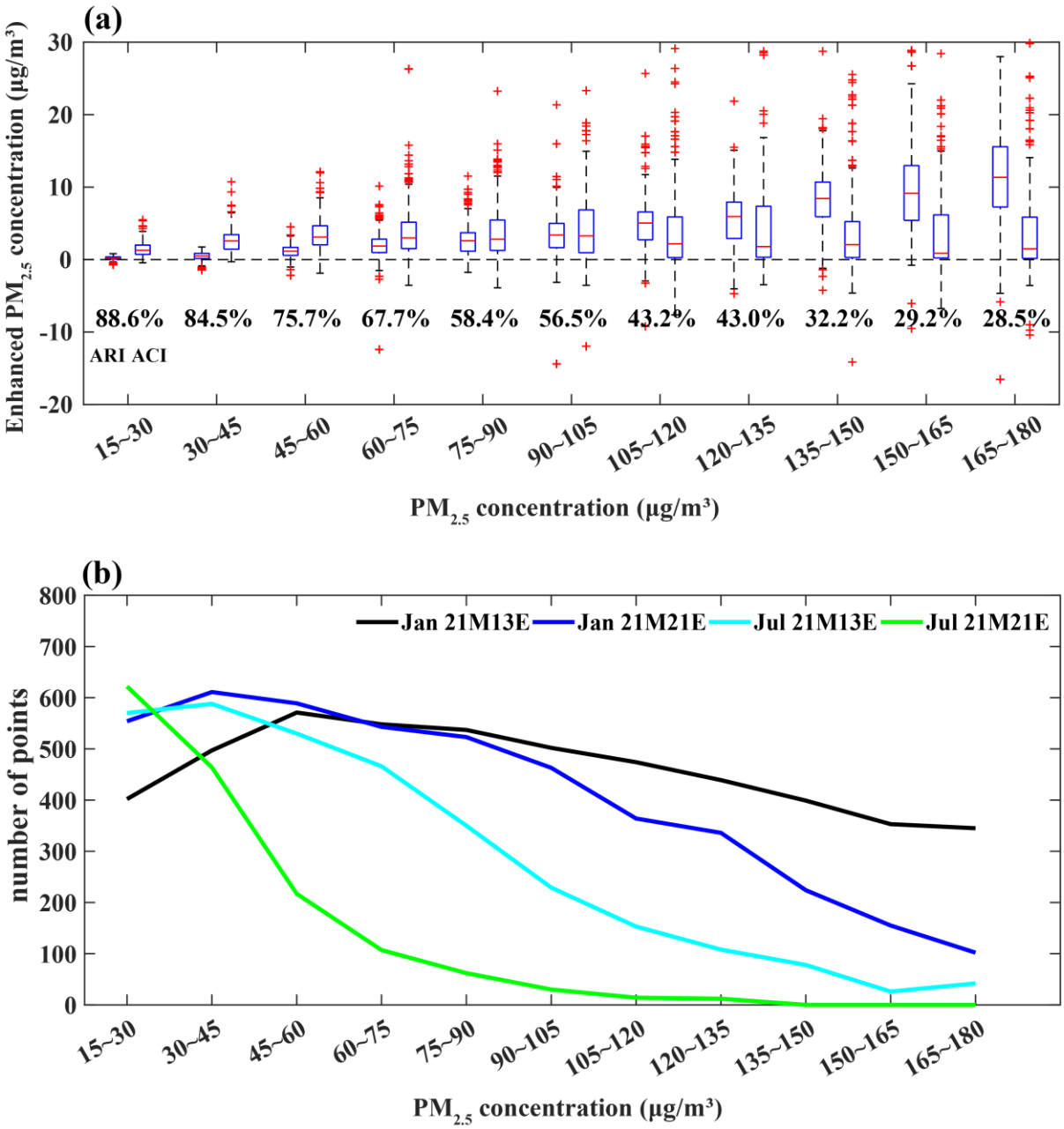

559

560 Fig. 5. (a) The enhanced $PM_{2.5}$ concentrations induced by ARI and ACI at
561 different ambient $PM_{2.5}$ levels. These data are from the simulations for January
562 and July in the experiments of 21M13E and 21M21E. The percentage represents
563 the ratio of the ACI-induced $PM_{2.5}$ enhancement to the sum of ARI- and ACI-
564 induced $PM_{2.5}$ enhancements. (b) The distributions of ambient $PM_{2.5}$ levels in
565 January and July in the experiments of 21M13E and 21M21E.

566

4. Conclusions

Under the background of sharped anthropogenic emission reduction, this study investigates changes of the ARI- and ACI-induced $PM_{2.5}$ enhancements for 2013–2021, and explores the causes for these changes from the perspectives of meteorological factors and $PM_{2.5}$ concentration distribution.

The results show that the enhanced $PM_{2.5}$ induced by the ARI (5.59 μg m^{-3}) is greater than that by the ACI (3.96 μg m^{-3}) in January 2013. However, the ARI- and ACI-induced $PM_{2.5}$ enhancements decrease from 5.59 and 3.96 μg m^{-3} to 1.37 and 1.93 μg m^{-3} in January and decrease by 75% and 51% for 2013–2021. The smaller decrease ratio (51%) for ACI-induced $PM_{2.5}$ enhancements implies that ACI becomes more important for enhancing $PM_{2.5}$ concentrations in January 2021. Furthermore, we separated the contributions of meteorological background variation and anthropogenic emission reduction. Compared with the meteorological background variation, anthropogenic emission reduction plays a more important role in causing the decrease of ARI- and ACI-induced $PM_{2.5}$ enhancements. Owing to only emission reduction, the enhanced $PM_{2.5}$ concentrations induced by the ARI and ACI decrease by 56% and 43% in January and 66% and 56% in July, respectively. The ACI-induced $PM_{2.5}$ enhancement becomes increasingly important in both January and July for 2013–2021. More specifically, the lower percentage decrease in the ACI-induced $PM_{2.5}$ enhancement is dominated by the lower decrease in the enhancements of secondary $PM_{2.5}$ components.

589 The lower percentage decrease in the enhanced $PM_{2.5}$ induced by the ACI is
590 due to the lower percentage decrease in the ACI-induced SWDOWN reduction,
591 which is because of the lower decrease in the LWP and increase in the Re caused
592 by the ambient $PM_{2.5}$ decrease in the high $PM_{2.5}$-polluted regime (Fig. 6). At the
593 same time, the lower percentage decreases in the T2 reduction and RH increase
594 induced by the ACI further lead to the lower percentage decrease in the
595 enhancements of the ACI-induced secondary $PM_{2.5}$ components (Fig. 6). Notably,
596 due to relative lower percentage decrease in the ACI-induced SWDOWN
597 reduction in the high $PM_{2.5}$-polluted regime, the increasing importance of ACI-
598 induced $PM_{2.5}$ enhancement is a matter of course with the ambient $PM_{2.5}$ decrease.
599

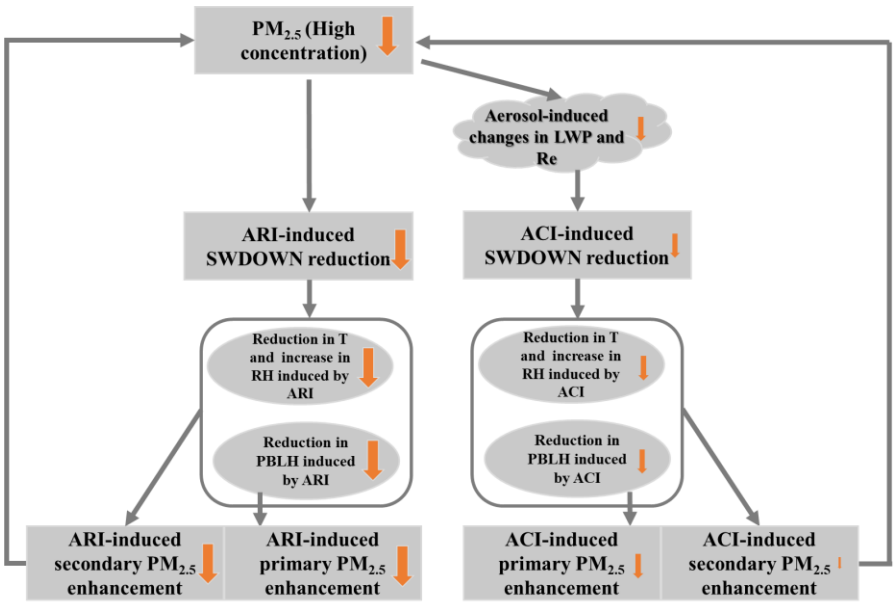

600

601 Fig. 6. Schematic diagram for the decrease of ARI- and ACI-induced primary and
602 secondary $PM_{2.5}$ enhancement due to reduction in ambient $PM_{2.5}$ concentration.
603 The size of the arrows represents the magnitude of changes due to reduction in
604 ambient PM2.5 concentration.

This study has important implication for the $PM_{2.5}$ control. As we know, ARI- and ACI-induced $PM_{2.5}$ enhancements have a non-negligible contribution to the deterioration of $PM_{2.5}$ air quality. Previous research has investigated the impact of anthropogenic emission reduction on the ARI-induced $PM_{2.5}$ enhancement (Zhou et al., 2019). But compared with $PM_{2.5}$ enhancement induced by ARI, that induced by ACI is more complicated and harder to be alleviated. Our findings have further revealed that the ACI-induced $PM_{2.5}$ enhancement is getting more important relative to that induced by ARI. This is especially true in cloud-prone areas like Sichuan-Chongqing area, which have witnessed rather weak decreases of ACI-induced $PM_{2.5}$ concentration in the past decade due to weak decreases of aerosol-induced LWP under the condition of high ambient $PM_{2.5}$ level (Fig. 2). The ACI-induced $PM_{2.5}$ enhancement needs to be considered more seriously in the formulation of control polices to meet national $PM_{2.5}$ air quality standard, especially in cloud-prone areas with high ambient $PM_{2.5}$ concentration. To control ACI-induced $PM_{2.5}$ enhancement, first, a larger emission reduction is necessary in cloudy areas compared with less cloudy areas to bring about a noticeable decrease in ACI-induced LWP in response to $PM_{2.5}$ reduction. Second, secondary inorganic aerosol (SNA), which is an important component of total aerosol, has a large influence on the ACI-induced $PM_{2.5}$ enhancement because of its high hygroscopicity. This makes it easy for SNA to be activated as CCN and influence LWP. We think that it is crucial to make

substantial decreases in the precursors of SNA, such as SO_2, NO_x and NH_3 species. These decreases could substantially decrease SNA. A large decrease in SNA would enhance the ACI-induced LWP response to $PM_{2.5}$ reduction and cause a large decrease in ACI-induced $PM_{2.5}$ enhancement. In addition, relative to ARI-induced $PM_{2.5}$ enhancement, the lower decrease in ACI-induced $PM_{2.5}$ enhancement is mainly because of the small decrease in ACI-induced enhancements of secondary $PM_{2.5}$ components. A substantial decrease in SNA would make the decrease ratio of ACI-induced $PM_{2.5}$ enhancement approach the more rapid decrease ratio of ARI-induced $PM_{2.5}$ enhancement.

Data and Code availability.

The data and code used in this study are available upon request from the corresponding author.

Author Contribution

D.G., B.Z. and S.W. designed the research; D.G., B.Z., J.S. and B.G. improved the WRF-Chem performance; D.G. and B.Z. performed WRF-Chem simulations; X.W., S.L. and Z.D. processed the anthropogenic emissions; D.G. analyzed the data with the help from B.Z., S.W. and Y.W.; D.Y. and J.S. helped to design some figures; S.W., Y.W., Y.Z. and Y.H. presented important suggestions for the analysis and writings; D.G. and B.Z. wrote the paper with inputs from all co-authors.

Competing interests

The author declares no competing interests.

Acknowledgments

This research is supported by the National Key Research and Development Program of China (2022YFC3701000, Task 5), the National Natural Science Foundation of China (22188102). We would like to thank Fenfen Zhang for providing the $PM_{2.5}$ components data for Handan city in January 2013.

References

Abdul-Razzak, H., and Ghan, S. J.: A parameterization of aerosol activation - 3. Sectional representation, J Geophys Res-Atmos, 107, Artn 4026 10.1029/2001jd000483, 2002.

Bellouin, N., Quaas, J., Gryspeerdt, E., Kinne, S., Stier, P., Watson-Parris, D., Boucher, O., Carslaw, K. S., Christensen, M., Daniau, A. L., Dufresne, J. L., Feingold, G., Fiedler, S., Forster, P., Gettelman, A., Haywood, J. M., Lohmann, U., Malavelle, F., Mauritsen, T., McCoy, D. T., Myhre, G., Mulmenstadt, J., Neubauer, D., Possner, A., Rugenstein, M., Sato, Y., Schulz, M., Schwartz, S. E., Sourdeval, O., Storelvmo, T., Toll, V., Winker, D., and Stevens, B.: Bounding Global Aerosol Radiative Forcing of Climate Change, Rev Geophys, 58, ARTN e2019RG000660 10.1029/2019RG000660, 2020.

671 Bennartz, R.: Global assessment of marine boundary layer cloud droplet number
672 concentration from satellite, J Geophys Res-Atmos, 112, Artn D02201
673 10.1029/2006jd007547, 2007.
674 Bougeault, P., and Lacarrere, P.: Parameterization Of Orography-Induced
675 Turbulence In a Mesobeta-Scale Model, Mon Weather Rev, 117, 1872-1890,
676 Doi 10.1175/1520-0493(1989)117<1872:Pooiti>2.0.Co;2, 1989.
677 Carter, W.: Documentation of the SAPRC-99 Chemical Mechanism for VOC
678 Reactivity Assessment, 2000.
679 Ding, A. J., Huang, X., Nie, W., Sun, J. N., Kerminen, V. M., Petaja, T., Su, H.,
680 Cheng, Y. F., Yang, X. Q., Wang, M. H., Chi, X. G., Wang, J. P., Virkkula,
681 A., Guo, W. D., Yuan, J., Wang, S. Y., Zhang, R. J., Wu, Y. F., Song, Y., Zhu,
682 T., Zilitinkevich, S., Kulmala, M., and Fu, C. B.: Enhanced haze pollution
683 by black carbon in megacities in China, Geophys Res Lett, 43, 2873-2879,
684 10.1002/2016GL067745, 2016.
685 Ding, D., Xing, J., Wang, S. X., Liu, K. Y., and Hao, J. M.: Estimated
686 Contributions of Emissions Controls, Meteorological Factors, Population
687 Growth, and Changes in Baseline Mortality to Reductions in Ambient
688 PM2.5 and PM2.5-Related Mortality in China, 2013-2017, Environ Health
689 Persp, 127, Artn 067009 10.1289/Ehp4157, 2019.
690 Donahue, N. M., Henry, K. M., Mentel, T. F., Kiendler-Scharr, A., Spindler, C.,
691 Bohn, B., Brauers, T., Dorn, H. P., Fuchs, H., Tillmann, R., Wahner, A.,
692 Saathoff, H., Naumann, K. H., Mohler, O., Leisner, T., Muller, L., Reinnig,

693 M. C., Hoffmann, T., Salo, K., Hallquist, M., Frosch, M., Bilde, M., Tritscher,
694 T., Barmet, P., Praplan, A. P., DeCarlo, P. F., Dommen, J., Prevot, A. S. H.,
695 and Baltensperger, U.: Aging of biogenic secondary organic aerosol via gas-
696 phase OH radical reactions, P Natl Acad Sci USA, 109, 13503-13508,
697 10.1073/pnas.1115186109, 2012.
698 Emery, C., Tai, E., Yarwood, G. : Enhanced meteorological modeling and
699 performance evaluation for two texas episodes, Report to the Texas Natural
700 Resources Conservation Commission, 2001.
701 Fan, J. W., Wang, Y., Rosenfeld, D., and Liu, X. H.: Review of Aerosol-Cloud
702 Interactions: Mechanisms, Significance, and Challenges, J Atmos Sci, 73,
703 4221-4252, 10.1175/Jas-D-16-0037.1, 2016.
704 Fast, J. D., Gustafson, W. I., Easter, R. C., Zaveri, R. A., Barnard, J. C., Chapman,
705 E. G., Grell, G. A., and Peckham, S. E.: Evolution of ozone, particulates, and
706 aerosol direct radiative forcing in the vicinity of Houston using a fully
707 coupled meteorology-chemistry-aerosol model, J Geophys Res-Atmos, 111,
708 Artn D21305 10.1029/2005jd006721, 2006.
709 Forkel, R., Werhahn, J., Hansen, A. B., McKeen, S., Peckham, S., Grell, G., and
710 Suppan, P.: Effect of aerosol-radiation feedback on regional air quality - A
711 case study with WRF/Chem, Atmos Environ, 53, 202-211,
712 10.1016/j.atmosenv.2011.10.009, 2012.
713 Forkel, R., Balzarini, A., Baro, R., Bianconi, R., Curci, G., Jimenez-Guerrero, P.,
714 Hirtl, M., Honzak, L., Lorenz, C., Im, U., Perez, J. L., Pirovano, G., San Jose,

715 R., Tuccella, P., Werhahn, J., and Zabkar, R.: Analysis of the WRF-Chem
716 contributions to AQMEII phase2 with respect to aerosol radiative feedbacks
717 on meteorology and pollutant distributions, Atmos Environ, 115, 630-645,
718 10.1016/j.atmosenv.2014.10.056, 2015.
719 Forster, P., T. Storelvmo, K. Armour, W. Collins, J.-L. Dufresne, D. Frame, D.J.
720 Lunt, T. Mauritsen, M.D. Palmer, M. Watanabe, M. Wild, and H. Zhang: The
721 Earth's Energy Budget, Climate Feedbacks, and Climate Sensitivity. In
722 Climate Change 2021: The Physical Science Basis. Contribution of Working
723 Group I to the Sixth Assessment Report of the Intergovernmental Panel on
724 Climate Change [Masson-Delmotte, V., P. Zhai, A. Pirani, S.L. Connors, C.
725 Péan, S. Berger, N. Caud, Y. Chen, L. Goldfarb, M.I. Gomis, M. Huang,
726 K. Leitzell, E. Lonnoy, J.B.R. Matthews, T.K. Maycock, T. Waterfield, O.
727 Yelekçi, R. Yu, and B. Zhou (eds.)], Cambridge, United Kingdom and New
728 York, NY, USA, Cambridge University Press, 923–1054, 2021.
729 Gao, M., Han, Z. W., Tao, Z. N., Li, J. W., Kang, J. E., Huang, K., Dong, X. Y.,
730 Zhuang, B. L., Li, S., Ge, B. Z., Wu, Q. Z., Lee, H. J., Kim, C. H., Fu, J. S.,
731 Wang, T. J., Chin, M., Li, M., Woo, J. H., Zhang, Q., Cheng, Y. F., Wang, Z.
732 F., and Carmichael, G. R.: Air quality and climate change, Topic 3 of the
733 Model Inter-Comparison Study for Asia Phase III (MICS-Asia III) - Part 2:
734 aerosol radiative effects and aerosol feedbacks, Atmos Chem Phys, 20,
735 1147-1161, 10.5194/acp-20-1147-2020, 2020.
736 Gong, W., Makar, P. A., Zhang, J., Milbrandt, J., Gravel, S., Hayden, K. L.,

737 Macdonald, A. M., and Leaitch, W. R.: Modelling aerosol-cloud-
738 meteorology interaction: A case study with a fully coupled air quality model
739 (GEM-MACH), Atmos Environ, 115, 695-715,
740 10.1016/j.atmosenv.2015.05.062, 2015.
741 Grell, G. A., and Freitas, S. R.: A scale and aerosol aware stochastic convective
742 parameterization for weather and air quality modeling, Atmos Chem Phys,
743 14, 5233-5250, 10.5194/acp-14-5233-2014, 2014.
744 Guenther, A., Karl, T., Harley, P., Wiedinmyer, C., Palmer, P. I., and Geron, C.:
745 Estimates of global terrestrial isoprene emissions using MEGAN (Model of
746 Emissions of Gases and Aerosols from Nature), Atmos Chem Phys, 6, 3181-
747 3210, DOI 10.5194/acp-6-3181-2006, 2006.
748 Gustafson, W. I., Chapman, E. G., Ghan, S. J., Easter, R. C., and Fast, J. D.:
749 Impact on modeled cloud characteristics due to simplified treatment of
750 uniform cloud condensation nuclei during NEAQS 2004, Geophys Res Lett,
751 34, Artn L19809 10.1029/2007gl030021, 2007.
752 Hong, C. P., Zhang, Q., Zhang, Y., Davis, S. J., Zhang, X., Tong, D., Guan, D. B.,
753 Liu, Z., and He, K. B.: Weakening aerosol direct radiative effects mitigate
754 climate penalty on Chinese air quality, Nat Clim Change, 10, 845-+,
755 10.1038/s41558-020-0840-y, 2020.
756 Iacono, M. J., Delamere, J. S., Mlawer, E. J., Shephard, M. W., Clough, S. A., and
757 Collins, W. D.: Radiative forcing by long-lived greenhouse gases:
758 Calculations with the AER radiative transfer models, J Geophys Res-Atmos,

113, Artn D13103 10.1029/2008jd009944, 2008.

Janjic, Z. I.: The Step-Mountain Eta Coordinate Model - Further Developments Of the Convection, Viscous Sublayer, And Turbulence Closure Schemes, Mon Weather Rev, 122, 927-945, Doi 10.1175/1520-0493(1994)122<0927:Tsmecm>2.0.Co;2, 1994.

Kanji, Z. A., Ladino, L. A., Wex, H., Boose, Y., Burkert-Kohn, M., Cziczo, D. J., and Kramer, M.: Overview of Ice Nucleating Particles, Meteor Mon, 58, 10.1175/Amsmonographs-D-16-0006.1, 2017.

Kong, X., Forkel, R., Sokhi, R. S., Suppan, P., Baklanov, A., Gauss, M., Brunner, D., Baro, R., Balzarini, A., Chemel, C., Curci, G., Jimenez-Guerrero, P., Hirtl, M., Honzak, L., Im, U., Perez, J. L., Pirovano, G., San Jose, R., Schlunzen, K. H., Tsegas, G., Tuccella, P., Werhahn, J., Zabkar, R., and Galmarini, S.: Analysis of meteorology-chemistry interactions during air pollution episodes using online coupled models within AQMEII phase-2, Atmos Environ, 115, 527-540, 10.1016/j.atmosenv.2014.09.020, 2015.

Le, T. H., Wang, Y., Liu, L., Yang, J. N., Yung, Y. L., Li, G. H., and Seinfeld, J. H.: Unexpected air pollution with marked emission reductions during the COVID-19 outbreak in China, Science, 369, 702-+, 10.1126/science.abb7431, 2020.

Li, L., An, J. Y., Zhou, M., Yan, R. S., Huang, C., Lu, Q., Lin, L., Wang, Y. J., Tao, S. K., Qiao, L. P., Zhu, S. H., and Chen, C. H.: Source apportionment of fine particles and its chemical components over the Yangtze River Delta, China

781 during a heavy haze pollution episode, Atmos Environ, 123, 415-429,
782 10.1016/j.atmosenv.2015.06.051, 2015.
783 Li, M., Zhang, Q., Kurokawa, J., Woo, J. H., He, K. B., Lu, Z. F., Ohara, T., Song,
784 Y., Streets, D. G., Carmichael, G. R., Cheng, Y. F., Hong, C. P., Huo, H.,
785 Jiang, X. J., Kang, S. C., Liu, F., Su, H., and Zheng, B.: MIX: a mosaic Asian
786 anthropogenic emission inventory under the international collaboration
787 framework of the MICS-Asia and HTAP, Atmos Chem Phys, 17, 935-963,
788 10.5194/acp-17-935-2017, 2017.
789 Li Shengyue, W. S., Wu Qingru: Emission trends of air pollutants and CO2 in
790 China from 2005 to 2021, Earth System Science Data,
791 https://doi.org/10.5194/essd-2022-464, 2023.
792 Lin, C. J.: Characteristics and Sources of Water-soluble Inorganic Ions in
793 Atmospheric Particulate Matter and Rainfall in the suburb of Mianyang,
794 Master, Southwest University of Science and Technology, 2022.
795 Liu, Q., Jia, X. C., Quan, J. N., Li, J. Y., Li, X., Wu, Y. X., Chen, D., Wang, Z. F.,
796 and Liu, Y. G.: New positive feedback mechanism between boundary layer
797 meteorology and secondary aerosol formation during severe haze events, Sci
798 Rep-Uk, 8, Artn 6095 10.1038/S41598-018-24366-3, 2018.
799 Liu, Y. Y., Xing, J., Wang, S. X., Fu, X., and Zheng, H. T.: Source-specific
800 speciation profiles of PM2.5 for heavy metals and their anthropogenic
801 emissions in China, Environ Pollut, 239, 544-553,
802 10.1016/j.envpol.2018.04.047, 2018.

Liu, S., Xing, J., Zhao, B., Wang, J. D., Wang, S. X., Zhang, X. Y., and Ding, A. J.: Understanding of Aerosol-Climate Interactions in China: Aerosol Impacts on Solar Radiation, Temperature, Cloud, and Precipitation and Its Changes Under Future Climate and Emission Scenarios, Curr Pollut Rep, 5, 36-51, 10.1007/s40726-019-00107-6, 2019.

Matthias, V., Aulinger, A., Bieser, J., Chen, Y. J., Geyer, B., Gao, J., Quante, M., and Zhang, F.: Modeling high aerosol loads in China in January 2013, Urban Clim, 22, 35-50, 10.1016/j.uclim.2016.04.005, 2017.

Moch, J. M., Mickley, L. J., Keller, C. A., Bian, H. S., Lundgren, E. W., Zhai, S. X., and Jacob, D. J.: Aerosol-Radiation Interactions in China in Winter: Competing Effects of Reduced Shortwave Radiation and Cloud-Snowfall-Albedo Feedbacks Under Rapidly Changing Emissions, J Geophys Res-Atmos, 127, ARTN e2021JD035442 10.1029/2021JD035442, 2022.

Morrison, H., Thompson, G., and Tatarskii, V.: Impact of Cloud Microphysics on the Development of Trailing Stratiform Precipitation in a Simulated Squall Line: Comparison of One- and Two-Moment Schemes, Mon Weather Rev, 137, 991-1007, 10.1175/2008MWR2556.1, 2009.

Myhre, G., Stordal, F., Johnsrud, M., Kaufman, Y. J., Rosenfeld, D., Storelvmo, T., Kristjansson, J. E., Berntsen, T. K., Myhre, A., and Isaksen, I. S. A.: Aerosol-cloud interaction inferred from MODIS satellite data and global aerosol models, Atmos Chem Phys, 7, 3081-3101, DOI 10.5194/acp-7-3081-2007, 2007.

825 Niu, G. Y., Yang, Z. L., Mitchell, K. E., Chen, F., Ek, M. B., Barlage, M., Kumar,
826 A., Manning, K., Niyogi, D., Rosero, E., Tewari, M., and Xia, Y. L.: The
827 community Noah land surface model with multiparameterization options
828 (Noah-MP): 1. Model description and evaluation with local-scale
829 measurements, J Geophys Res-Atmos, 116, Artn D12109
830 10.1029/2010jd015139, 2011.
831 Rosenfeld, D., Sherwood, S., Wood, R., and Donner, L.: Climate Effects of
832 Aerosol-Cloud Interactions, Science, 343, 379-380,
833 10.1126/science.1247490, 2014.
834 Savane, O. S., Vant-Hull, B., Mahani, S., and Khanbilvardi, R.: Effects of Aerosol
835 on Cloud Liquid Water Path: Statistical Method a Potential Source for
836 Divergence in Past Observation Based Correlative Studies, Atmosphere-
837 Basel, 6, 273-298, 10.3390/atmos6030273, 2015.
838 Seinfeld, J. H., Bretherton, C., Carslaw, K. S., Coe, H., DeMott, P. J., Dunlea, E.
839 J., Feingold, G., Ghan, S., Guenther, A. B., Kahn, R., Kraucunas, I.,
840 Kreidenweis, S. M., Molina, M. J., Nenes, A., Penner, J. E., Prather, K. A.,
841 Ramanathan, V., Ramaswamy, V., Rasch, P. J., Ravishankara, A. R.,
842 Rosenfeld, D., Stephens, G., and Wood, R.: Improving our fundamental
843 understanding of the role of aerosol-cloud interactions in the climate system,
844 P Natl Acad Sci USA, 113, 5781-5790, 10.1073/pnas.1514043113, 2016.
845 Shrivastava, M., Fast, J., Easter, R., Gustafson, W. I., Zaveri, R. A., Jimenez, J.
846 L., Saide, P., and Hodzic, A.: Modeling organic aerosols in a megacity:

847 comparison of simple and complex representations of the volatility basis set
848 approach, Atmos Chem Phys, 11, 6639-6662, 10.5194/acp-11-6639-2011,
849 2011.
850 Wang, J. D., Wang, S. X., Jiang, J. K., Ding, A. J., Zheng, M., Zhao, B., Wong,
851 D. C., Zhou, W., Zheng, G. J., Wang, L., Pleim, J. E., and Hao, J. M.: Impact
852 of aerosol-meteorology interactions on fine particle pollution during China's
853 severe haze episode in January 2013, Environ Res Lett, 9, Artn 094002
854 10.1088/1748-9326/9/9/094002, 2014.
855 Wang, Z. F., Li, J., Wang, Z., Yang, W., Tang, X., Ge, B., Yan,P., Zhu, L., Chen,
856 X., and Chen, H.: Modeling study of regional severe hazes over mid-eastern
857 China in January 2013 and its implications on pollution prevention and
858 control, Science China Earth Sciences, 3-13,
859 https://doi.org/10.1007/s11430-013-4793-0, 2014.
860 Wang, H., Shi, G. Y., Zhang, X. Y., Gong, S. L., Tan, S. C., Chen, B., Che, H. Z.,
861 and Li, T.: Mesoscale modelling study of the interactions between aerosols
862 and PBL meteorology during a haze episode in China Jing-Jin-Ji and its near
863 surrounding region - Part 2: Aerosols' radiative feedback effects, Atmos
864 Chem Phys, 15, 3277-3287, 10.5194/acp-15-3277-2015, 2015.
865 Wang, L. W., Wen, L., Xu, C. H., Chen, J. M., Wang, X. F., Yang, L. X., Wang,
866 W. X., Yang, X., Sui, X., Yao, L., and Zhang, Q. Z.: HONO and its potential
867 source particulate nitrite at an urban site in North China during the cold
868 season, Sci Total Environ, 538, 93-101, 10.1016/j.scitotenv.2015.08.032,

2015.

Wang, J. D., Zhao, B., Wang, S. X., Yang, F. M., Xing, J., Morawska, L., Ding, A. J., Kulmala, M., Kerminen, V. M., Kujansuu, J., Wang, Z. F., Ding, D. A., Zhang, X. Y., Wang, H. B., Tian, M., Petaja, T., Jiang, J. K., and Hao, J. M.: Particulate matter pollution over China and the effects of control policies, Sci Total Environ, 584, 426-447, 10.1016/j.scitotenv.2017.01.027, 2017.

Wang, Y. S., Li, W. J., Gao, W. K., Liu, Z. R., Tian, S. L., Shen, R. R., Ji, D. S., Wang, S., Wang, L. L., Tang, G. Q., Song, T., Cheng, M. T., Wang, G. H., Gong, Z. Y., Hao, J. M., and Zhang, Y. H.: Trends in particulate matter and its chemical compositions in China from 2013-2017, Sci China Earth Sci, 62, 1857-1871, 10.1007/s11430-018-9373-1, 2019.

Wild, O., Zhu, X., and Prather, M. J.: Fast-j: Accurate simulation of in- and below-cloud photolysis in tropospheric chemical models, J Atmos Chem, 37, 245-282, Doi 10.1023/A:1006415919030, 2000.

Wu, J. R., Bei, N. F., Hu, B., Liu, S. X., Wang, Y., Shen, Z. X., Li, X., Liu, L., Wang, R. N., Liu, Z. R., Cao, J. J., Tie, X. X., Molina, L. T., and Li, G. H.: Aerosol-photolysis interaction reduces particulate matter during wintertime haze events, P Natl Acad Sci USA, 117, 9755-9761, 10.1073/pnas.1916775117, 2020.

Xiong, C. R., Li, J., Liu, Z. X., and Zhang, Z. Y.: The dominant role of aerosol-cloud interactions in aerosol-boundary layer feedback: Case studies in three megacities in China, Front Env Sci-Switz, 10, Artn 1002412

10.3389/Fenvs.2022.1002412, 2022.

Xue, C. Y., Zhang, C. L., Ye, C., Liu, P. F., Catoire, V., Krysztofiak, G., Chen, H., Ren, Y. G., Zhao, X. X., Wang, J. H., Zhang, F., Zhang, C. X., Zhang, J. W., An, J. L., Wang, T., Chen, J. M., Kleffmann, J., Mellouki, A., and Mu, Y. J.: HONO Budget and Its Role in Nitrate Formation in the Rural North China Plain, Environ Sci Technol, 54, 11048-11057, 10.1021/acs.est.0c01832, 2020.

Zaveri, R. A., Easter, R. C., Fast, J. D., and Peters, L. K.: Model for Simulating Aerosol Interactions and Chemistry (MOSAIC), J Geophys Res-Atmos, 113, Artn D13204 10.1029/2007jd008782, 2008.

Zhang, B., Wang, Y., and Hao, J.: Simulating aerosol-radiation-cloud feedbacks on meteorology and air quality over eastern China under severe haze conditions in winter, Atmos Chem Phys, 15, 2387-2404, 10.5194/acp-15-2387-2015, 2015.

Zhang, F. F.: Characteristics of Air Pollution and Chemical Composition of PM2.5 in Handan Master, College of Urban Construction, Hebei University of Engineering, 2015.

Zhang, X., Zhang, Q., Hong, C. P., Zheng, Y. X., Geng, G. N., Tong, D., Zhang, Y. X., and Zhang, X. Y.: Enhancement of PM2.5 Concentrations by Aerosol-Meteorology Interactions Over China, J Geophys Res-Atmos, 123, 1179-1194, 10.1002/2017JD027524, 2018.

Zhang, F., Wang, Y., Peng, J. F., Chen, L., Sun, Y. L., Duan, L., Ge, X. L., Li, Y.

X., Zhao, J. Y., Liu, C., Zhang, X. C., Zhang, G., Pan, Y. P., Wang, Y. S., Zhang, A. L., Ji, Y. M., Wang, G. H., Hu, M., Molina, M. J., and Zhang, R. Y.: An unexpected catalyst dominates formation and radiative forcing of regional haze, P Natl Acad Sci USA, 117, 3960-3966, 10.1073/pnas.1919343117, 2020.

Zhang, F. F., Xing, J., Ding, D. A., Wang, J. D., Zheng, H. T., Zhao, B., Qi, L., and Wang, S. X.: Role of black carbon in modulating aerosol direct effects driven by air pollution controls during 2013-2017 in China, Sci Total Environ, 832, ARTN 154928 10.1016/j.scitotenv.2022.154928, 2022.

Zhao, C., Liu, X., Leung, L. R., Johnson, B., McFarlane, S. A., Gustafson, W. I., Fast, J. D., and Easter, R.: The spatial distribution of mineral dust and its shortwave radiative forcing over North Africa: modeling sensitivities to dust emissions and aerosol size treatments, Atmos Chem Phys, 10, 8821-8838, 10.5194/acp-10-8821-2010, 2010.

Zhao, C., Chen, S., Leung, L. R., Qian, Y., Kok, J. F., Zaveri, R. A., and Huang, J.: Uncertainty in modeling dust mass balance and radiative forcing from size parameterization, Atmos Chem Phys, 13, 10733-10753, 10.5194/acp-13-10733-2013, 2013.

Zhao, B., Liou, K. N., Gu, Y., Li, Q. B., Jiang, J. H., Su, H., He, C. L., Tseng, H. L. R., Wang, S. X., Liu, R., Qi, L., Lee, W. L., and Hao, J. M.: Enhanced PM2.5 pollution in China due to aerosol-cloud interactions, Sci Rep-Uk, 7, Artn 4453 10.1038/S41598-017-04096-8, 2017.

935 Zheng, H. T., Cai, S. Y., Wang, S. X., Zhao, B., Chang, X., and Hao, J. M.:
936 Development of a unit-based industrial emission inventory in the Beijing-
937 Tianjin-Hebei region and resulting improvement in air quality modeling,
938 Atmos Chem Phys, 19, 3447-3462, 10.5194/acp-19-3447-2019, 2019.
939 Zhou, M., Zhang, L., Chen, D., Gu, Y., Fu, T. M., Gao, M., Zhao, Y. H., Lu, X.,
940 and Zhao, B.: The impact of aerosol-radiation interactions on the
941 effectiveness of emission control measures, Environ Res Lett, 14, Artn
942 024002 10.1088/1748-9326/Aaf27d, 2019.